Chemical Dynamics Simulations of CO2 in the Ground and First Excited Bend States Colliding with a Perfluorinated Self-Assembled Monolayer

ARTICLE *in* THE JOURNAL OF PHYSICAL CHEMISTRY C · OCTOBER 2010

Impact Factor: 4.77 · DOI: 10.1021/jp103511g

5 AUTHORS, INCLUDING:

Juan J. Nogueira
University of Vienna
15 PUBLICATIONS **81** CITATIONS
SEE PROFILE

Saulo A Vázquez
University of Santiago de Compostela
90 PUBLICATIONS **1,048** CITATIONS
SEE PROFILE

Upakarasamy Lourderaj
The National Institute of Science Educatio…
26 PUBLICATIONS **532** CITATIONS
SEE PROFILE

Chemical Dynamics Simulations of CO_2 in the Ground and First Excited Bend States Colliding with a Perfluorinated Self-Assembled Monolayer

J. J. Nogueira,[†] S. A. Vázquez,[†] U. Lourderaj,[‡] W. L. Hase,[§] and E. Martínez-Núñez*,[†]

Departamento de Química Física y Centro Singular de Investigación en Química Biológica y Materiales Moleculares, Universidad de Santiago de Compostela, 15782 Santiago de Compostela, Spain, School of Chemical Sciences, National Institute of Science Education and Research, Bhubaneswar 751005, India, and Department of Chemistry and Biochemistry, Texas Tech University, Lubbock, Texas 79409, United States

Received: April 19, 2010; Revised Manuscript Received: July 23, 2010

Energy transfer in collisions of CO_2, in the ground (00^00) state and first excited (01^10) bend state, with a perfluorinated alkanethiol self-assembled monolayer (F-SAM) was studied by quasiclassical trajectory simulations employing a united-atom (UA) model to represent the F-SAM. The CO_2 molecule was aimed perpendicularly to the surface at incident energies of 1.6 and 10.6 kcal/mol. The exchange of bend energy is more efficient for penetrating trajectories while almost no energy exchange was found for direct trajectories. Bend energy transfer depends on the surface residence time (τ). In particular, the average bend energy of the scattered CO_2 molecules increases linearly with τ for $CO_2(00^00)$ + F-SAM, and it decreases linearly for $CO_2(01^10)$ + F-SAM at both incident energies. For the highest collision energy, the average bend energy of the scattered CO_2 molecules also increases linearly with the angle formed between the molecular axis and the axis perpendicular to the surface in $CO_2(00^00)$ + F-SAM collisions. The J quantum number distributions $P(J)$ of the scattered CO_2 molecules in the (00^00) and (01^10) states compare very well with experimental results of CO_2 scattering off a perfluorinated liquid surface. Finally, the computed vibrational populations also compare well with the experimental distributions, providing vibrational temperatures below the surface temperature. The analysis of the computed vibrational temperatures as a function of the residence time provide us with a value of ~50 ps for the time scale needed to achieve vibrational energy accommodation.

Introduction

Experimental studies of interactions between a gas and a liquid surface have provided us with fundamental knowledge of the scattering mechanism.[1−14] Recently, Nesbitt's group has investigated in detail the dynamics of collisions of CO_2 with liquid surfaces.[15−22] Distributions of the scattered CO_2 molecules for the vibrational, rotational, and translational degrees of freedom help elucidate the scattering mechanism, for example, whether it is dominated by thermal-desorption (TD) or by higher energy, nonthermal desorption. In particular, Nesbitt and co-workers studied the stereodynamics,[15,18,19] the influence of the incident angle,[16,20] of the collision energy,[21] and of the surface temperature,[17] on the collision dynamics of CO_2 with perfluoropolyether (PFPE) and with perfluorinated alkanethiol self-assembled monolayers (F-SAM) on gold using dynamics simulations.

The results of Nesbitt and co-workers on the CO_2 + PFPE scattering dynamics provide evidence for nonthermal scattering dynamics. In particular, the CO_2 rotational distributions are consistent with two different mechanisms: a thermal desorption (TD) Boltzmann component in which the scattered molecules become accommodated with the 298 K surface temperature and a component with much higher energies and a Boltzmann temperature of ~750 K.[22] The experimental results also show that CO_2 scatters off the liquid surface in both the ground (00^00) state and the first excited (01^10) bend state, with vibrational temperatures T_{vib} in the range 200−300 K, i.e., much colder than T_{rot}, and below the liquid surface temperature of 298 K. The inefficient warming of the CO_2 bend mode is in accordance with standard theories of energy transfer among different degrees of freedom, whereby impulsive collisions can impart considerable additional energy into translation and rotation, while the vibrational states with much larger energy spacings remain largely unpopulated. In contrast to rotation and translation motion, the bend vibrational mode of CO_2 appears to be largely decoupled from the surface, at least on time scales sampled under the experimental scattering conditions. To reach equilibrium, CO_2 must remain on the surface sufficiently long to exchange 667 cm^{-1} (1.9 kcal/mol) of energy into and/or out of the bending vibrational manifold. Similar results were found in experimental studies of acetylene (C_2H_2) scattering from LiF(100).[23] The results indicate that acetylene largely retains its vibrational energy throughout the scattering event and the time required to completely relax the vibrations of acetylene was much longer than needed to translationally accommodate the molecules with the surface. No experimental or theoretical studies of vibrational relaxation have been performed for CO_2 physisorbed on a PFPE liquid or similar surface. Therefore, it would be of interest to carry out dynamics simulations of vibrational energy accommodation in collisions of CO_2 with PFPE or F-SAM.

We have studied the dynamics of collisions of CO_2 with F-SAM[24,25] and compared the simulation results with those obtained by Nesbitt and co-workers in their experiments of CO_2 scattering off a liquid PFPE surface.[22] The simulations identify three different trajectory types, i.e., those that penetrate the surface, physisorb on the top of the surface, and directly scatter

* To whom correspondence should be addressed.
[†] Universidad de Santiago de Compostela.
[‡] National Institute of Science Education and Research.
[§] Texas Tech University.

10.1021/jp103511g
Published on Web 10/13/2010

without penetration or physisorption. Of these trajectory types only those that penetrate are accommodated with the 298 K surface temperature. The calculated CO_2 rotational energy distribution is in near quantitative agreement with experiment and may be fit by a sum of Boltzmanns as is done experimentally. However, an analysis of the trajectories indicates that the low temperature, 298 K, Boltzmann component is comprised of all three trajectory types. The translational energy distribution of the scattered CO_2 molecules is also determined from the simulations and it may not be fit by the sum of two Boltzmanns as is possible for the rotational energy distribution.

Although the surfaces used in the experiments and in the simulations are different, experiment and simulations predict similar internal energy distributions of the scattered CO_2 molecules. This suggests that F-SAM can be used as a model surface in energy transfer studies of CO_2 scattering off a liquid PFPE surface. The use of F-SAM as a model for liquid PFPE to study the scattering dynamics of CO_2 molecules is further supported by work done in Cooks's group,[26] who observed similar energy transfer efficiencies and ion-surface reactions for both PFPE and F-SAM, and by Ramsamy and Pradeep,[27] who observed that the surface of PFPE is primarily formed by the terminal $-CF_3$ groups.

In the present work, chemical dynamics simulations of CO_2 in the ground (00^00) and first excited (01^10) bend states scattering from F-SAM are performed to study vibrational relaxation/warming of the bend vibrational mode in the scattering process. Comparisons are made with the available experimental rovibrational CO_2 distributions of the scattered molecules at two incident energies, 1.6 and 10.6 kcal/mol.[21,22] Our goal is to study in detail the exchange of energy into and/or out of the bending vibrational manifold and to determine the time scale for vibrational energy accommodation.

Computational Details

A. Potential Energy Surfaces. The potential function for the system has been described previously,[25] and comprises an intramolecular potential for carbon dioxide, V_{CO_2}, a potential for the F-SAM, V_{surf}, and the interaction between both, V_{CO_2-surf}:

$$V = V_{CO_2} + V_{surf} + V_{CO_2-surf} \quad (1)$$

In previous work,[28] several united atom (UA) models for the F-SAM were developed, where the CF_3 and CF_2 groups are treated as single pseudoatoms. With this simplification the total number of interaction sites diminishes dramatically with respect to the all atom (AA) model,[24,25] which results in a substantial decrease in CPU time. Among the UA models proposed in our previous work,[28] UA3 gives the best results for energy transfer efficiencies and for rotational and translational distributions of the scattered CO_2 molecules. The good performance of UA3 alongside with the considerable save in CPU time (simulations using the UA models of the F-SAM are ~3 times faster than those using the corresponding AA models) made it our choice for the simulations presented in this paper.

As in previous computational studies,[24,25,28] the F-SAM surface consists of 48 chains of $CF_3(CF_2)_7S$ radicals adsorbed on a single layer of 196 constrained Au atoms. The potentials for CO_2, for the surface and the interaction between both are described in previous work[28] and for simplicity there are not given here. Figure 1 shows the 48 UA chains that make up the model for our F-SAM with the definition of the coordinates and angle used below. In particular, X and Y define the surface plane, Z is the surface normal and β is the angle formed between the O−O direction (z) and the Z axis.

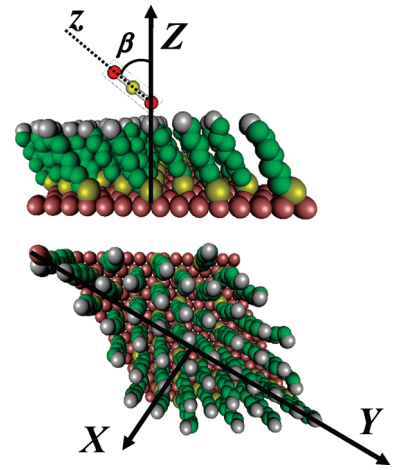

Figure 1. UA model of the F-SAM with the 48 chains and the definition of the coordinates and angles used in this study.

B. Trajectory Simulations. Carbon dioxide molecules collide with the surface perpendicularly (along the Z axis) with incident energies of 1.6 and 10.6 kcal/mol. The dynamics of CO_2 scattering from PFPE at both incident energies were investigated experimentally.[21] The projectiles are aimed randomly at a point in the unit cell on the surface as described in detail in previous work.[25] The initial separation between CO_2 and the surface aiming point was 25 Å (37 Å above the gold atoms). Prior to the propagation of the first trajectory, a molecular dynamics simulation was performed for 2 ps to ensure thermal relaxation of the F-SAM surface at 298 K. The structure thus obtained was used later as the initial structure of a 100 fs equilibration run before the second trajectory. This process was repeated before initiation of each trajectory. Periodic boundary conditions and the image vector convention[29] were used to represent a larger surface, thus avoiding possible complications that may appear in collisions resulting in multiple CO_2 encounters with the surface. Trajectories were stopped when the distance between CO_2 and the surface was 30 Å or when 150 ps elapsed. The Adams−Moulton algorithm was employed to integrate the trajectories with a fixed step size of 0.3 fs. With this step size the energy conservation was better than five significant figures. For each of the initial conditions, batches of 5000 trajectories were run with VENUS05.[30]

Internal Energy Sampling of CO_2. The aim of this work is to obtain an insight into the vibrational activation/relaxation processes of vibrationally cold/excited carbon dioxide colliding with an F-SAM. The lowest frequency mode of CO_2 is the degenerate bend modes ($\tilde{\nu} = 667$ cm^{-1}). Excitations of the degenerate bends thus provide a good opportunity to investigate vibrational energy transfer between carbon dioxide and the surface. In addition, Nesbitt and co-workers in their experiments of CO_2 scattering off PFPE[21] reported vibrational temperatures of the incident beam of the order of ~200 K, which populates the first excited bend state (01^10) of CO_2. The vibrational state of carbon dioxide is denoted as (n_1,N^L,n_3), where n_1, N, n_3, and L are the symmetric stretch, the degenerate bends, the asymmetric stretch, and the vibrational angular momentum quantum numbers, respectively.

In the present work, chemical dynamics simulations were performed for the two lowest bend states of CO_2, (00^00) and (01^10). Since we are only interested in the CO_2 bend energy, and the vibrational quantum numbers of the stretchings (n_1 and

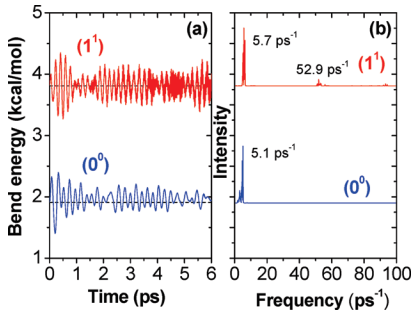

Figure 2. (a) Average bend energies vs time for an ensemble of 100 trajectories of CO_2 in the (0^0) and (1^1) bend states (blue and red lines, respectively). (b) Fourier transforms of the average bend energies of plot (a) for the corresponding initial states.

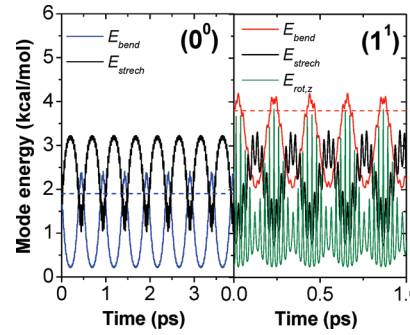

Figure 3. Mode energies for individual trajectories of CO_2 in their (0^0) and (1^1) bend states. Black lines correspond to the symmetric stretch energies. Blue and red lines correspond to the bend energies in the (0^0) and (1^1) states, respectively, and the green line is the rotational energy about the molecular axis (z).

n_3) are zero, the notation (N^L) instead of ($0N^L0$) will be used throughout the paper for simplicity. Therefore, according to the vibrational frequencies of our model potential[25] the symmetric and asymmetric stretching modes have energies of 1.81 and 3.46 kcal/mol, respectively.

The sampling of vibrational angular momemtum states for linear molecules has been presented elsewhere[31] and is already one of the standard options of VENUS05. Briefly, the sampling assumes the harmonic oscillator and separable rotation-vibration model, for which the total energy for a linear molecule's pair of normal-mode degenerate bends is

$$E_{\text{bend}} = \left(n_a + \frac{1}{2}\right)h\nu + \left(n_b + \frac{1}{2}\right)h\nu = (N+1)h\nu \quad (2)$$

where the n's are the bends' vibrational quantum numbers and $N = n_a + n_b$. Each value of N is associated with $N + 1$ degenerate energy levels and wave functions $\Psi(n_a,n_b)$ corresponding to different possible combinations of n_a and n_b. The vibrational angular momenta for the states are $j_z = L\hbar$, (z is the axis of the molecule) with $L = N, N-2, ..., -(N-2), -N$. By changing the difference in the phase of the two degenerate bends, a given vibrational angular momentum quantum number L can be selected. Details of this algorithm have been given previously.[31] The initial rotational quantum number J was set to 0 in our calculations.

Some of the initial bend energy of CO_2 could flow to the symmetric stretch due to the strong coupling between both modes. This energy flow is expected to be fast in comparison with the time needed to reach the F-SAM surface (~2.5 ps at $E_i = 10.6$ kcal/mol).[24] To investigate intramoleclar vibrational energy transfer in our model for CO_2, the average bending energies for ensembles of 100 trajectories were calculated as a function of time. Figure 2a shows these average mode energies for the (0^0) and (1^1) states. The bend energies show fluctuations due to energy transfer processes between the various modes of the molecule, although the time averaged value is conserved in the time scale shown in the figure. The Fourier transform (FT) of the average bend energies yield a spectrum that contains bands at frequencies corresponding to the mode-to-mode rate coefficients.[32] Figure 2b shows the FT of the corresponding energies in panel a. The FT of the (0^0) state shows only one band at 5.1 ps^{-1}, which corresponds to the rate at which the energy is being transferred between the bending mode and the symmetric stretch. For the (1^1) state there is an additional band with very low intensity at 52.9 ps^{-1} that involves the rotation about the molecular axis, initially excited in the (1^1) state. The two mode-to-mode energy transfer rates 5.1 and 52.9 ps^{-1} correspond to very short time scales of 0.2 and 0.02 ps, respectively; much shorter than the time needed for CO_2 to reach the F-SAM (at least 2.5 ps).

Although the average vibrational bend energy is conserved for several ps for an ensemble of trajectories as seen above, this may not be the case for individual trajectories. In particular, Figure 3 shows, for an individual trajectory, the bending and symmetric stretching energies and the rotational energy about the molecular axis for the (0^0) and (1^1) states of CO_2. As seen in the figure, the initial energy of the (0°) state (1.9 kcal/mol) is not conserved for this trajectory and it drops to an average value of 1.0 kcal/mol; the energy difference of 0.9 kcal/mol between the initial and the time averaged value is transferred to the symmetric stretch. For the (1^1) state there is also a drop in the bending energy although in this case it only represents ~20% of its initial value (the initial bending energy is 3.8 kcal/mol and the average value after several ps is 3.0 kcal/mol). For the (1^1) state, excitation of the vibrational angular momentum is conserved, which prevents a dramatic energy flow to the stretching mode as occurred for the (0^0) state. The nonconservation of the mode energies poses an important complication in the present study.

The unphysical bend energy leakage can be largely attenuated by selecting only those trajectories that conserve their time averaged mode energies within a reasonable percentage of the initial value. Ensembles of 10^5 trajectories were run to investigate the conditions for which the (0^0) and (1^1) bend states conserve their energy. The trajectories that conserved their bend energies were found to fulfill a particular relationship between the phases of the stretching and bending normal modes. In particular, it was found that when the phase of the bending mode α_b and that of the stretching α_s follow this relationship:

$$\alpha_s = (a - n)\pi + b\alpha_b \quad (3)$$

the conservation of the time averaged bending mode energy is within 3% of its initial value. The phases of both the bending and stretching modes are depicted in Figure 4 for those trajectories with (0^0) that conserve their bend energies. The quasiperiodic character of the CO_2 trajectories can be studied by the so-called Poincaré surface of section,[33] which is constructed by plotting simultaneous (θ, $d\theta/dt$) values whenever the trajectory crosses a given line ($R_{CO} = R_{CO}^{eq}$ in our case). The resulting points provide snapshots of the underlying phase space orbits. Figure 5 shows the Poincaré surfaces of section for four different CO_2 trajectories, for the (0^0) bend state, with time

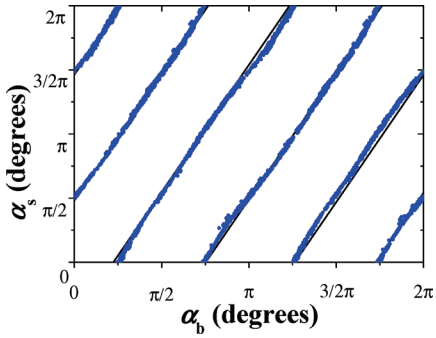

Figure 4. Correlations between the phase of the stretching mode (α_s) and that of the bending mode (α_b) for the trajectories that conserve their average bend energy within 3% of its initial value in the (0^0) state.

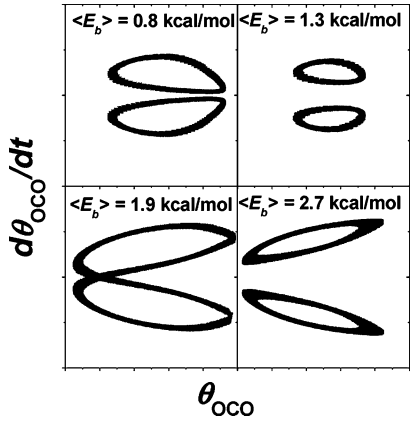

Figure 5. Poincaré surfaces of section (for dθ/dt vs θ, where θ is the OCO angle) calculated for four different CO_2 trajectories with $N = 0$ and $L = 0$. The symmetric stretching contains the zero-point energy and the asymmetric stretch has no energy. The total integration time was 50 ps. The surfaces-of-section were obtained for $R_{CO} = R_{CO}^{eq}$.

averaged bend mode energies of 0.8, 1.3, 1.9, and 2.7 kcal/mol. The integration time was 50 ps, and since the asymmetric stretching is not coupled with the other modes, it was given no energy in these simulations. Our calculations confirm that all trajectories with the same time averaged bend mode energies have the same Poincaré surfaces of section. The Poincaré surfaces of section for those trajectories that conserve their initial energy in the bend mode (1.9 kcal/mol) are distorted eights, whereas trajectories with different time averaged bend mode energies give rise to different patterns as seen in the Figure. All trajectories are quasiperiodic for the (0^0) bend state but the initial phase differences between the bending and the stretching give rise to different bend mode energies and phase space orbits.

For the (1^1) state a similar behavior of the stretching and bending phases was found and the results of the fits of eq 3 to the trajectory points are collected in Table 1. In the fittings the values of a were fixed and b and n were optimized. First, for each initial bend state, six initial fits were done for each group of points in Figure 4. Then, using the average values of b, eq 3 was refit to the trajectory data, fixing now both a and b, and optimizing the values of n. The percentage of trajectories that conserve their initial energies is 3% and 10% for the (0^0) and (1^1) states, respectively. Therefore, the algorithm that selects vibrational angular states for linear molecules in VENUS[31] was modified for CO_2 to restrict the phases of the symmetric stretch according to eq 3. In a section below, the use of eq 3 to select the initial normal mode phases of the CO_2 molecules is discussed in more detail.

TABLE 1: Parameters Obtained in the Fits of eq 3 to the Trajectory Data That Show the Relationship between the Phases of the Stretching and Bending Modes for Trajectories That Conserve Their Bend Energies

CO_2 bend state	a	b^a	n^b
(0^0)	1.5	1.982 ± 0.008	0.003 ± 0.009
			1.016 ± 0.001
			1.977 ± 0.002
			2.985 ± 0.002
			3.945 ± 0.002
			4.929 ± 0.003
(1^1)	1.6	2.016 ± 0.009	0.055 ± 0.003
			0.935 ± 0.004
			1.985 ± 0.003
			2.925 ± 0.003
			3.973 ± 0.002
			4.886 ± 0.006

[a] The reported errors for b are the average errors of each of the fits in the first fitting (see text). [b] Each value of n corresponds to the different lines of Figure 4.

Determination of the Final CO_2 Energies and Rovibrational States. From the final coordinates and momenta of CO_2, internal (rotational and vibrational) and bend mode energies can be obtained. The procedure to calculate the internal energies is standard in VENUS05. Since the internal coordinates do not depend on the molecular frame, they can be employed to calculate the bend energy as described by Wilson et al.[34] In particular, for CO_2 the bend energy can be calculated from the values of its angle θ and its time derivative dθ/dt as

$$E_{\text{bend}} = \frac{1}{2} f_\theta (\theta - \theta_e)^2 + \frac{1}{2} \frac{m_O m_C R_e^2}{2m_C + 4m_O} \dot{\theta}^2 + \frac{j_z^2}{2I_z} \quad (4)$$

where m_O, m_C, and R_e are the masses of the oxygen and carbon atoms and the CO equilibrium distance, respectively; f_θ is the bending force constant and I_z the moment of inertia about the molecular axis.

A real value for the bend vibrational state N can be determined by equating eq 2 to the classical determination of the bending energy [eq 4] and L and J can be determined from the relationships $j_z = L\hbar$ and $j = [J(J + 1)]^{1/2}\hbar$, respectively. The usual procedure to get integer values (quantum numbers) from the above classical actions consists in rounding the real values to the nearest integer [hereinafter called histogram binning (HB)], so that each trajectory will contribute 0 or 1 to the probability to end in a given quantum number. Some years ago, Bonnet and Rayez[35,36] proposed the use of Gaussian functions centered in the integer values (quantum numbers) to get more reliable distributions in the products. Gaussian binning (GB) was found to be superior than HB in predicting reactive cross sections and product energy distributions for a number of processes.[37−40] In the GB, each trajectory will contribute to the probability of every quantum number n but will contribute more for values of the classical actions close to n. In the present work, the final N and L quantum numbers of CO_2 were assigned according to both the HB and the GB. The full-width-half-maximum (fwhm) of the Gaussian functions was 0.5 in the GB. Previous studies by Aoiz and co-workers[37−40] used narrower Gaussian functions. However, decreasing the fwhm of the Gaussians is not possible in our study due to poor statistics around the (1^1) state. For an accurate analysis of our trajectory results using GB, the total number of trajectories should be significantly increased. For this reason, the results obtained in

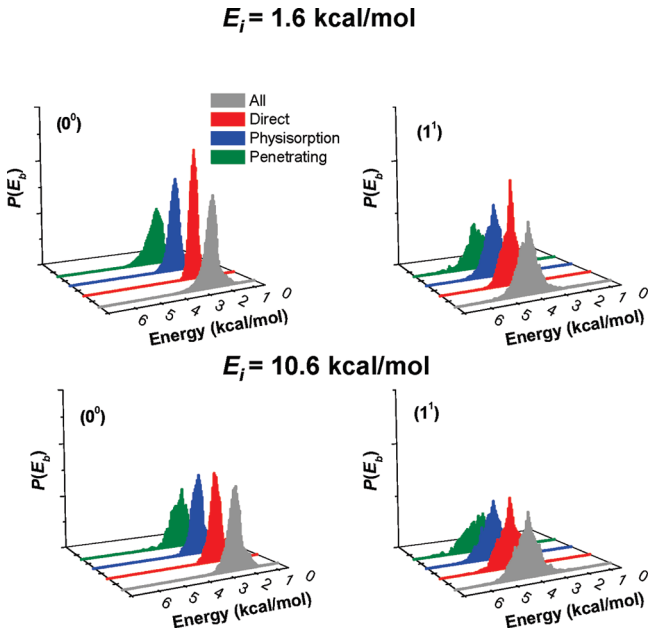

Figure 6. Distributions of the bend energy $P(E_b)$ for the different trajectory types at the incident energies and initial bend states studied here. The energy is calculated according to eq 4 and therefore refers to the bottom of the well.

this study with GB should be taken with caution and regarded only as an alternative to HB.

Results

A. Bend Energy Transfer. The distributions of the final bend energies $P(E_b)$ of the scattered CO_2 molecules are depicted graphically in Figure 6 for both the (0^0) and (1^1) initial states at the two incident energies studied here. The colored areas in the figure represent the distributions for the different trajectory types. The percentages of (direct, penetration and physisorption) trajectories for the (0^0) initial state are (14, 33, and 53) and (46, 14, and 40) at $E_i = 1.6$ and 10.6 kcal/mol, respectively. These values are the same for the bend excited state. The differences in the percentages of the trajectory types as a function of incident energy have been discussed in detail previously.[24]

In addition, Table 2 collects the full-width at half-maximum (fwhm) and the average bend energy $\langle E_b \rangle$. The $P(E_b)$ distributions for the (0^0) initial state at both incident energies are slightly hot with an average value of 2.0 kcal/mol (vs an initial bend energy of 1.9 kcal/mol). The (0^0) $P(E_b)$ distributions of the penetrating trajectories (green color) are broad with a fwhm of ~1.0 kcal/mol vs 0.6 kcal/mol obtained for the remaining trajectories (see Table 2). Additionally, the average value of the bend energy $\langle E_b \rangle$ of the penetrating trajectories (for the initial 0^0 state) is 2.1 vs 2.0 kcal/mol obtained for all trajectories. This indicates that bend energy transfer is more efficient for penetrating trajectories than for the remaining trajectories.

The $P(E_b)$ distributions found in our study for both incident energies are very similar except those for the direct trajectories at $E_i = 1.6$ kcal/mol, which are narrower than the others. For the initial (0^0) state, the fwhm is only 0.4 kcal/mol. Direct trajectories undertake only one inner turning point along the Z direction,[24] which inefficiently promotes vibrational energy transfer. In addition, at the lowest incident energy, energy transfer is inefficient by an impulsive mechanism as well, which explains the almost 100% adiabatic behavior of the bend energy for direct trajectories.

The trajectories for the initial (1^1) state present broader distributions than those for for the (0^0) state; the FWHMs for the (1^1) state are 0.2−0.5 kcal/mol higher than those for the (0^0) state. Additionally, the penetrating trajectories give rise to $P(E_b)$ distributions with a fwhm of 1.3 (1.6) for $E_i = 1.6$ kcal/mol (10.6 kcal/mol) (much higher than those for the remaining trajectories). The average values of the $P(E_b)$ distributions for the (1^1) state are about 3.7 kcal/mol for both incident energies. For the penetrating trajectories the average values of the distributions are lower than those for the remaining trajectories. As above, bend energy transfer is more efficient for penetrating trajectories.

In previous work, we had found that penetrating trajectories led to rotational and translational distributions of the scattered CO_2 molecules which could be fit by 298 K (the surface temperature) Boltzmann distributions.[24,25] This result indicates that the time scale involved in the penetration process is long enough to ensure rotational and translational energy accommodation, which is in line with our conclusion that bend energy transfer is more efficient for penetrating trajectories. To investigate whether the time scale of penetration is also enough to attain vibrational energy accommodation, the dependence of the $P(E_b)$ distributions for the penetrating trajectories with the residence time was also analyzed. As in previous work,[24] the residence time τ is defined here as the difference between the first and the last inner turning points in the Z direction. Figure 7 shows the variation of $\langle E_b \rangle$ for the penetrating trajectories as a function of τ for the two incident energies and initial states. To obtain $\langle E_b \rangle$, the trajectories were sorted in different bins so that every bin has a similar number of trajectories. As seen in the figure, $\langle E_b \rangle$ increases as a function of τ for the (0^0) state, whereas it decreases for the excited state. The average bend energies follow the same behavior for both incident energies.

TABLE 2: Features of the Final Bend Energy Distributions $P(E_b)$ at the Two Incident Energies Studied Here

initial state		direct	physisorption	penetration	total
		$E_i = 1.6$ kcal/mol			
(0^0)	fwhm[a]	0.41 ± 0.00	0.53 ± 0.00	0.97 ± 0.02	0.57 ± 0.01
	$\langle E_b \rangle$[a]	1.95 ± 0.01	2.02 ± 0.01	2.12 ± 0.03	2.05 ± 0.01
(1^1)	fwhm	0.69 ± 0.01	0.83 ± 0.01	1.34 ± 0.03	0.90 ± 0.01
	$\langle E_b \rangle$	3.75 ± 0.02	3.74 ± 0.02	3.64 ± 0.04	3.72 ± 0.02
		$E_i = 10.6$ kcal/mol			
(0^0)	fwhm	0.59 ± 0.01	0.64 ± 0.01	1.02 ± 0.02	0.64 ± 0.01
	$\langle E_b \rangle$	2.00 ± 0.01	2.02 ± 0.01	2.11 ± 0.04	2.02 ± 0.01
(1^1)	fwhm	0.98 ± 0.02	1.05 ± 0.01	1.58 ± 0.03	1.06 ± 0.01
	$\langle E_b \rangle$	3.73 ± 0.02	3.76 ± 0.02	3.63 ± 0.06	3.74 ± 0.02

[a] In kcal/mol. The FWHMs are obtained from fits of Gaussian functions to our $P(E_b)$ distributions. The reported errors are given for a 95% confidence limit.

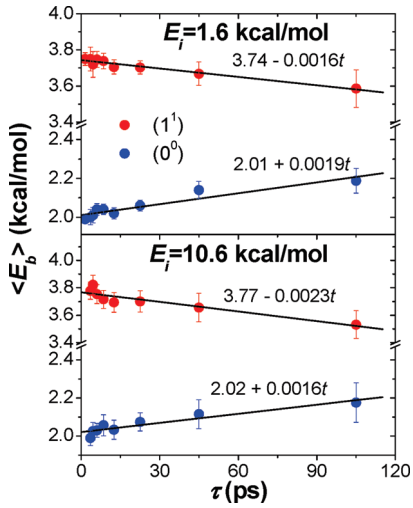

Figure 7. Variation of the average bend energies $\langle E_b \rangle$ vs residence time (τ) for the incident energies and initial bend states studied here.

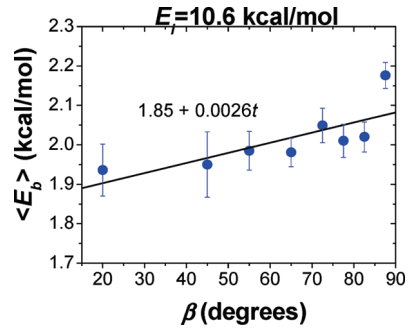

Figure 8. Variation of the average bend energies $\langle E_b \rangle$ vs the angle β, formed between the CO_2 molecular axis (z) and Z (see Figure 1), for the incident energies and initial bend states studied here.

As seen in the figure, the bend energy shows linear dependence on the residence time on the time interval studied here 0−120 ps. However, this linear dependence is very weak (the slopes of the fits are ≤0.002 kcal/mol/ps) and, it seems that the time scale needed for vibrational energy accommodation is very long. This will be discussed in detail below.

The dependence of the vibrational angular momentum, j_z, on τ was also studied here, although the plots are not shown for simplicity. The average vibrational angular momentum increases with τ for the (0^0) ensemble of trajectories and it decreases for the (1^1) trajectories, following the same behavior as the bend energy.

The dependence of the average bend energy on the angle β formed between the CO_2 molecular axis (z) and Z at the moment of impact (see Figure 1 for the definition) was also investigated. As seen in Figure 8, it was found that, for the (0^0) initial state at E_i = 10.6 kcal/mol, $\langle E_b \rangle$ increases with β for the direct trajectories. For the other incident energy and bend states no angle dependence was found. As above, to calculate $\langle E_b \rangle$ the trajectories were sorted in different bins so that every bin has similar number of trajectories. For perpendicular orientations of CO_2 with respect to the surface ($\beta = 0^0$) there is negligible excitation of the bend mode, whereas for $\beta = 90^0$ (with the CO_2 molecular axis lying on the XY plane) there is maximum excitation of the bend mode. This behavior can be explained on the basis of the hard-cube model[41] for gas-surface energy transfer, which rests on the assumption that the tangential component of momentum of the gas is conserved during collision with the surface, or, in other words, that the forces between the gas and the surface lie along the Z axis. Thus, in collisions with $\beta = 0^0$ the forces exerted on the molecule lie along the molecular axis, which is perpendicular to the bend mode eigenvector, whereas for $\beta = 90^0$ the forces exerted on the molecule are parallel to the bend mode eigenvector, making excitation of the bend mode possible, provided the forces on the different atoms are different. This effect is not seen for E_i = 1.6 kcal/mol, because the magnitude of the forces is much smaller than for E_i = 10.6 kcal/mol. Hynes and co-workers found, in their study on the vibrational relaxation of the C−Cl bond of methyl chloride in water, that orientation of the water molecules with respect to the C−Cl bond is crucial and only those molecules that collide perpendicular to the C−Cl bond contribute significantly to the relaxation of the bond.[42]

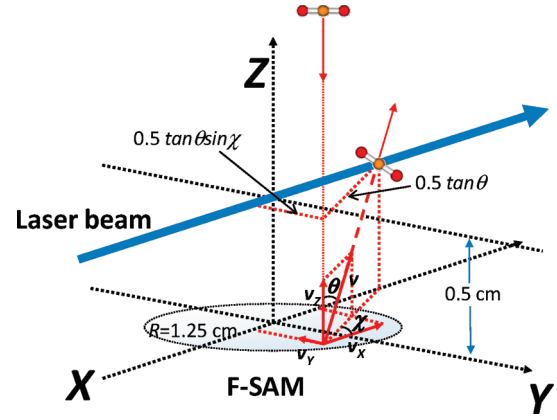

Figure 9. Laser beam geometry used in the experiments of Nesbitt and co-workers.[21,22] The laser propagation is assumed to be along the X axis and passes 0.5 cm above the F-SAM surface. The scattering (θ) and azymuthal (χ) angles serve to sort the molecules according to whether they cross the laser beam and should be included in the analysis or not.

B. Comparison with Experiment: Flux-to-Density Transformation and Laser Geometry. The simulation results of the present study are compared in this section with recent experimental work in Nesbitt's group for CO_2 scattering off PFPE.[21,22] In previous work, we have already shown that F-SAM is a very good model for PFPE to study the scattering dynamics of carbon dioxide.[24,25]

To carry out a detailed comparison between our simulations and the experiments, one has to take into account that the simulations provide flux distributions, where each trajectory has the same weight, and the 3D scattering space has no restrictions. However, in the experimental measurements, the concentration of CO_2 molecules in the laser volume (density) rather than flux is determined. In addition, the experimental laser geometry is very important because some projectiles scattering off the surface might not cross the laser beam depending on their final scattering and azymuthal angles.

Therefore, in order to make a rigorous comparison between simulations and experiments, the laser geometry has to be taken into account and flux-to-density transformations have to be made beforehand. The laser geometry employed by Perkins and Nesbitt,[21,22] is depicted in the cartoon of Figure 9, where the laser beam is assumed to be parallel to the X axis. In particular, the laser beam is passed above a spot where the molecular beam strikes the surface. The spot is represented in the figure as a circle of 2.5 cm of diameter and the laser is about 0.5 cm above the surface. Assuming uniform coverage over the collision area, only those CO_2 molecules that fulfill the following relationship between their scattering θ and azymuthal χ angles

$$\chi < \arcsin\left(\frac{2.5}{\tan\theta}\right) \tag{5}$$

will reach the laser beam and be detected. Therefore in our comparison of the trajectory results with the experiments only those trajectories that fulfill eq 5 are counted.

Additionally, the probability of absorption is proportional to the time the molecule would spend traversing the laser beam. To carry out the flux-to-density transformation the laser beam is assumed to be a cylinder of diameter D. The transit time τ across the laser beam can be therefore calculated according to

$$\tau = \frac{D}{\sqrt{v_Y^2 + v_Z^2}} \tag{6}$$

Since D is constant for each trajectory, the weight of each individual trajectory is just τ/D. This flux-to-density transformation was found to provide very good results for the J-dependent translational energy distributions of CO_2.[24]

The first comparison between our simulations and the experiments concerns the distributions $P(J)$ of the rotational quantum number J of the CO_2 molecules ending in the (0^0) and (1^1) bend states. As in previous work,[24,25] the $P(J)$ distributions obtained in our simulations were fit to the sum of two components, low temperature (LT) and high temperature (HT)

$$P(J) = \alpha_{LT}P_{LT} + \alpha_{HT}P_{HT} \tag{7}$$

where each of normalized component is given by

$$P_X(J) = \frac{(2J+1)\exp(-E_{rot}/kT_{rot}(X))}{Q_{rot}(X)} \tag{8}$$

with X = LT or HT. The rotational temperature of the LT component was fixed to 298 K, with α_{LT} and T_{rot}(HT) being the only variable parameters during the fittings.

Figure 10 displays graphically the distributions calculated in this work in comparison with the experimental data (circles) for the final (0^0) and (1^1) states of CO_2. The simulation results correspond to the fits of eq 7 to the trajectory data for the two incident energies using both GB and HB. Nesbitt and co-workers found that the population of the final (1^1) state is only 0.03 that of the (0^0) state,[22] however both distributions are normalized to one for visual clarity. The difference in the population of the (0^0) and (1^1) states explains the scattering in the experimental data for the final (1^1) state. The general conclusion from the figure is that the differences between the HB and GB theoretical results are negligible and both results agree well with the experimental data. The percentages of LT and HT components and their associated temperatures are collected in Table 3 for each of the distributions. The theoretical distributions at E_i = 1.6 kcal/mol are all well fit by single Boltzmann distributions with temperatures very close to the surface temperature. The experimental distribution for the (0^0) final state gives essentially the same result. At the highest E_i, the distributions are bimodal with each component (LT and HT) contributing approximately 50%. The rotational temperature of the HT component in our distributions for the final (0^0) state is about 770−800 K, which agrees, within the errors of the fits, with the experimental value of 710 K ± 60 K. Both the (0^0) and (1^1) manifolds present very similar $P(J)$ distributions.

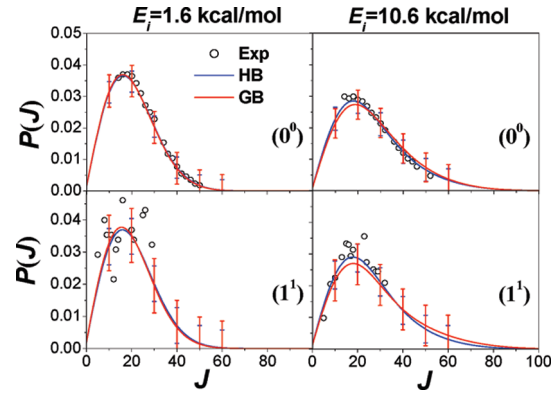

Figure 10. $P(J)$ distributions obtained in our simulations with HB and GB for the final (0^0) and (1^1) states of CO_2 compared with the experimental data (circles) at the two incident energies. The errors of the fits are given for the 95% confidence limits every 10 units.

TABLE 3: Parameters of the $P(J)$ Distributions Obtained in the Fits to the Trajectory Data at E_i = 10.6 kcal/mol as a Function of the Final N^L State of CO_2

final state		α_{LT}	T_{rot} (LT)	T_{rot} (HT)
		E_i = 1.6 kcal/mol		
(0^0)	HB	1	304 ± 5	
	GB	1	299 ± 7	
	exp[a]	0.92 ± 0.12	298	330 ± 100
(1^1)	HB	1	299 ± 7	
	GB	1	286 ± 1	
		E_i = 10.6 kcal/mol		
(0^0)	HB	0.52 ± 0.04	298	806 ± 64
	GB	0.42 ± 0.05	298	769 ± 67
	exp[a]	0.54 ± 0.03	298	710 ± 60
(1^1)	HB	0.53 ± 0.05	298	773 ± 78
	GB	0.51 ± 0.05	298	980 ± 125

[a] From ref 21.

The second comparison between our simulations and experiment concerns the population analysis of the (N^L) states of the scattered CO_2 molecules. The resulting percentages of molecules ending in a particular (N^L) state are collected in Tables 4 and 5 for E_i = 1.6 and 10.6 kcal/mol, respectively. The vibrational temperatures collected in the tables are "two-point" estimates using the (0^0) and (1^1) populations.

In all cases, HB and GB give similar results with the distributions obtained with HB being slightly hotter than those obtained with GB. For the trajectories with (1^1) initial bend states at both incident energies, the (2^2) state is populated after collision, but not the (2^0) state, which indicates that vibrational angular momentum is, in general, excited upon collisions with the F-SAM. This result has been already found in previous work and used to explain the apparent zero-point energy leakage of CO_2.[25]

All vibrational temperatures found in our simulations are near or below the surface temperature. To obtain vibrational temperatures from our simulations that can be compared with those obtained in the experiments, no more calculations are needed. In particular, the final bend state populations of the trajectories with (0^0) and (1^1) initial bend states (see Tables 4 and 5) were weighted by the ratio of populations of both states obtained from the vibrational temperatures of the molecular beam: 255 and 190 K at E_i = 1.6 and 10.6 kcal/mol, respectively. The results collected in Tables 4 and 5 agree very well with the experimental data. In particular, at E_i = 1.6 kcal/mol the vibrational temperature obtained experimentally is 295 K, which compares

TABLE 4: Quantum Distributions of the N^L States of Scattered CO_2 Obatined in Our Simulations at $E_i = 1.6$ kcal/mol in Comparison with the Experimental Results[a]

initial state		(0^0)	(1^1)	(2^0)	(2^2)	T_{vib}
(0^0)	HB	98.3 ± 0.7	1.7 ± 0.7	0.0	0.0	202
		93.0 ± 2.8	*7.0 ± 2.8*	*0.0*	*0.0*	*292*
	GB	99.5 ± 0.6	0.5 ± 0.6	0.0	0.0	163
		97.0 ± 3.2	*3.0 ± 3.2*	*0.0*	*0.0*	*230*
(1^1)	HB	3.7 ± 1.1	94.7 ± 1.3	0.0	1.6 ± 0.8	
		12.1 ± 3.9	*83.3 ± 4.6*	*0.0*	*4.6 ± 2.8*	
	GB	1.8 ± 1.3	97.6 ± 1.5	0.0	0.6 ± 0.7	
		8.5 ± 6.6	*89.2 ± 7.3*	*0.0*	*2.3 ± 3.5*	
experimental conditions[b]	HB	94.1 ± 0.7	5.9 ± 0.7	0.0	0.0	277
		89.5 ± 2.9	*10.3 ± 2.8*	*0.0*	*0.2*	*337*
	GB	95.1 ± 0.6	4.9 ± 0.6	0.0	0.0	262
		93.1 ± 3.4	*6.8 ± 3.2*	*0.0*	*0.1*	*290*
	exp	92.8	7.2			295

[a] Values in italic are for the penetrating trajectories. [b] The vibrational temperature of the moleculer beam is 255 K. The errors are given for the 95% confidence limits.

TABLE 5: Quantum Distributions of the N^L States of Scattered CO_2 Obatined in Our Simulations at $E_i = 10.6$ kcal/mol in Comparison with the Experimental Results[a]

initial state		0^0	1^1	2^0	2^2	T_{vib}
(0^0)	HB	99.4 ± 0.6	0.6 ± 0.6	0.0	0.0	164
		97.0 ± 3.8	*3.0 ± 3.8*	*0.0*	*0.0*	*230*
	GB	99.8 ± 0.5	0.2 ± 0.5	0.0	0.0	141
		98.0 ± 4.6	*2.0 ± 4.6*	*0.0*	*0.0*	*205*
(1^1)	HB	5.8 ± 1.6	92.1 ± 2.0	0.0	2.1 ± 1.3	
		20.6 ± 8.1	*75.9 ± 8.9*	*0.0*	*3.5 ± 4.8*	
	GB	2.9 ± 1.5	96.2 ± 1.9	0.0	0.9 ± 1.2	
		14.8 ± 10.3	*83.5 ± 11.2*	*0.0*	*1.7 ± 4.9*	
experimental conditions[b]	HB	98.3 ± 0.6	1.7 ± 0.6	0.0	0.0	202
		96.1 ± 3.9	*3.9 ± 3.8*	*0.0*	*0.0*	*247*
	GB	98.6 ± 0.5	1.4 ± 0.5	0.0	0.0	195
		97.1 ± 4.7	*2.9 ± 4.6*	*0.0*	*0.0*	*227*
	exp	97.0	3.0			230

[a] Values in italic are for the penetrating trajectories. [b] The vibrational temperature of the moleculer beam is 190 K. The errors are given for the 95% confidence limits.

quite well with the values obtained in our study of 262 and 272 K using GB and HB, respectively (see Table 4). At $E_i = 10.6$ kcal/mol the simulation results are 195 and 202 K for GB and HB, respectively, in comparison with a vibrational temperature of 230 K obtained experimentally (see Table 5). The vibrational temperature of the scattered CO_2 molecules obtained experimentally for the lowest incident energy (295 K) is higher than that obtained at the highest incident energy (230 K). However, the initial population of the (1^1) bend state at the lowest incident energy is higher than that for the highest incident energy due to different molecular beam conditions; the inefficient vibrational cooling in the experiments does not allow to draw a general conclusion.

The final populations of the (0^0) and (1^1) states obtained for the direct and physisorption trajectories are very similar to those obtained for the whole set of trajectories. However, the distributions for the penetrating trajectories are markedly different and are also collected in Tables 4 and 5 for comparison. The vibrational distributions of the penetrating trajectories are hotter than those obtained for the remaining trajectories. In particular, the vibrational distribution of the penetrating trajectories for the initial (0^0) state at $E_i = 1.6$ kcal/mol obtained with HB gives a vibrational temperature of 292 K, very close to the surface temperature of 298 K, and the result for GB is 230 K. For the other trajectory types (direct and physisorption), vibrational energy accommodation does not take place in the time scales of these processes. In particular, for the initial (0^0) state, the direct trajectories at $E_i = 10.6$ kcal/mol (not shown in the tables) show a final population of the (0^0) state of 100% (99.9%) using HB(GB); for $E_i = 1.6$ kcal/mol the final population of the (0^0) state is 100% for both binning procedures. The results for the physisorption trajectories are almost identical to those obtained for the whole set of trajectories. The average time scales for direct and physisorption trajectories are 0 and 10 ps, respectively.[24]

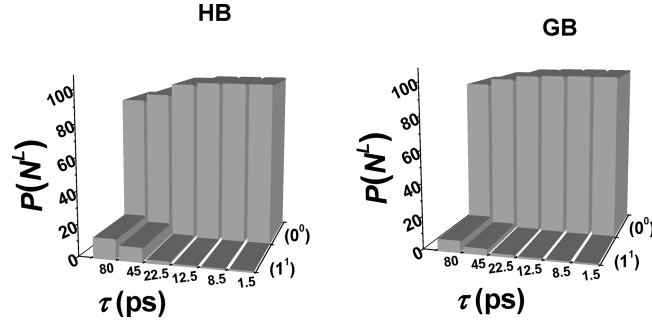

Figure 11. Distributions of the final (0^0) and (1^1) states as a function of residence time (τ) for the penetrating trajectories of the ensemble at $E_i = 1.6$ kcal/mol and (0^0) initial bend state.

Our simulation results agree with the experimental evidence of a lack of appreciable thermalization of the bend at $E_i = 10.6$ kcal/mol.[17] In order to quantify the time needed to achieve vibrational energy accommodation, Figure 11 shows the final populations of the (0^0) and (1^1) states of CO_2 for trajectories with initial (0^0) bend states at $E_i = 1.6$ kcal/mol as a function of the residence time for both HB and GB. The trajectories were

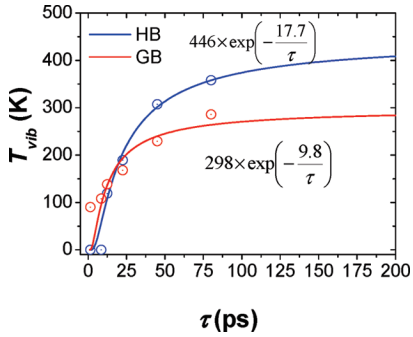

Figure 12. Dependence of the vibrational temperature (calculated from the (0^0) and (1^1) final populations of Figure 10) as a function of residence time (τ) using HB and GB.

sorted in different bins so that every bin has a similar number of trajectories. Although the HB vibrational distributions are slightly hotter than those obtained with GB, both distributions are very cold (with the final (0^0) state having a probability ≥99%) for residence times lower than 25 ps.

The vibrational temperatures calculated using the final populations of the (0^0) and (1^1) states are depicted graphically in Figure 12 as a function of the residence time at $E_i = 1.6$ kcal/mol. The behavior of the vibrational temperature (T_{vib}) vs τ is asymptotic and the following equation fits reasonably the $T_{vib}(\tau)$ plots

$$T_{vib}(\tau) = a \exp\left(-\frac{b}{\tau}\right) \quad (9)$$

As seen in Figure 12, the fitting of eq 9 to the HB temperatures is better than that to the GB temperatures. The value of parameter a, which is the limiting vibrational temperature for infinite residence time is 298 K for the GB temperatures (red circles) and 446 K for the HB temperatures (blue circles). The limiting vibrational temperature obtained with GB surprisingly coincides with the surface temperature and that obtained with HB is higher. The latter result is clearly in error due to the approximations used to obtain the vibrational populations and temperatures. Anyway, as seen in Figure 12, more than 50 ps are needed to reach vibrational temperatures close to the surface temperature (298 K). This time scale is an order of magnitude higher than that found by Hynes and co-workers in their study on the relaxation of the 670 cm^{-1} C−Cl vibration of CH_3Cl in water.[42] However, methyl chloride is a dipolar molecule in a polar solvent and the Coulombic solute−solvent interactions accelerate the relaxation of the C−Cl vibration.

C. Accuracy of the Results and the Surface Model. The bend mode energies of the scattered CO_2 molecules may be affected, as the incoming ones, by the artificial bend energy leakage commented above. However, as seen in Figure 3, the drop of the bend mode energy occurs in the very first fs, after which the energy in the bend mode oscillates around a constant average value. This means that, for the scattered molecules, this unphysical bend−stretch energy flow takes place when the intermolecular forces are still playing an important role in the dynamics. For this reason, it is not possible to know the amount of bend energy that leaked to/from the stretch mode for the scattered molecules. On the other hand, the use of eq 3 to select the initial normal mode phases is intended to correct the unphysical energy flow due to the normal mode sampling. Since the sampling is not exact, the symmetric stretching is expected to receive some excitation in the process. The scattered molecules are free of this problem.

In order to investigate the effect of constraining the initial normal mode phases of the CO_2 molecules, an additional batch of 5000 trajectories was run using all CO_2 molecules (without selecting individual trajectories according to eq 3) at $E_i = 10.6$ kcal/mol. The resulted populations of the final 0^0 and 1^1 bend mode states of CO_2 are 96.0 (99.4) and 4.0 (0.6) using HB (GB), which follow the same trend as those of Table 5: 99.4 (99.8) and 0.6 (0.2) using HB (GB). The bend mode states populations obtained when the normal mode phases are not restricted are slightly hotter than those obtained using eq 3 for the incoming CO_2 molecules. However, this does not change the main conclusion of the manuscript that vibrational energy exchange is very inefficient.

Finally, to make sure that the UA model used does not introduce any artifacts in the simulations, an all atom model for the surface was used[25] for a batch of additional 5000 trajectories at $E_i = 10.6$ kcal/mol. The results for the final 0^0 and 1^1 bend mode states of CO_2 are 96.0 (98.2) and 4.0 (1.8) using HB (GB), which compare reasonably well with the UA results of Table 5. Again the main conclusion of the present work does not depend on the model used for the surface.

Conclusions

Chemical dynamics simulations were performed to study the dynamics of ground state and vibrationally excited CO_2 scattering off an F-SAM. Two different bend states of carbon dioxide were studied, the ground-state and the (01^10) excited state at incident energies of 1.6 and 10.6 kcal/mol to compare with the experimental results of Nesbitt and co-workers.[21,22] The simulation results show that energy transfer to/from the bend energy is more efficient for penetrating trajectories than for the remaining types of trajectories at the two incident energies studied here. Collisions with the CO_2 molecular axis (z) perpendicular to the surface normal (Z) tend to excite the bend mode more than do collisions with both axes parallel. The vibrational temperatures obtained in our study from the final bending mode quantum numbers are below the surface temperature and agree reasonably well with those obtained experimentally. This result suggests that bend energy energy accommodation takes place on a time scale longer than involved in the collision process. An analysis of the vibrational temperatures as a function of residence time shows that the time scale needed to achieve bend energy accommodation is at least 50 ps.

Finally, the J quantum number distributions $P(J)$ of the scattered CO_2 molecules compare very well with experiment at the two incident energies and for both bend states (00^00 and 01^10). At the lowest incident energy the theoretical results are fit by a single Boltzmann distributions with temperatures close to 298 K, whereas at the highest incident energy the $P(J)$ are bimodal with approximately equal contribution of the low-temperature and high-temperature components. The $P(J)$ distributions obtained in our study for both the ground state and first excited states of the bend mode of CO_2 are very similar to each other.

Acknowledgment. We acknowledge Javier Aoiz, Bradford G. Perkins and David J. Nesbitt for helpful discussions. S.A.V. and E.M.N. thank "Xunta de Galicia" for financial support ("Axuda para a Consolidación e Estructuración de unidades de investigación competitivas do Sistema Universitario de Galicia, 2007/50, cofinanciada polo FEDER 2007−2013″ and Grant No. PGDIT07PXIB209072PR) and "Ministerio de Educación y

Ciencia" (Grant No. CTQ2009-12588). The research by U.L. and W.L.H. was supported by the National Science Foundation under Grant No. OISE-0730114 and the Robert A. Welch Foundation under Grant No. D-0005.

References and Notes

(1) Saecker, M. E.; Govoni, S. T.; Kowalski, D. V.; King, M. E.; Nathanson, G. M. *Science* **1991**, *252*, 1421.

(2) Kenyon, A. J.; McCaffery, A. J.; Quintella, C. M.; Zidan, M. D. *Chem. Phys. Lett.* **1992**, *190*, 55.

(3) Saecker, M. E.; Nathanson, G. M. *J. Chem. Phys.* **1993**, *99*, 7056.

(4) King, M. E.; Nathanson, G. M.; Hanning-Lee, M. A.; Minton, T. K. *Phys. Rev. Lett.* **1993**, *70*, 1026.

(5) Saecker, M. E.; Nathanson, G. M. *J. Chem. Phys.* **1994**, *100*, 3999.

(6) King, M. E.; Saecker, M. E.; Nathanson, G. M. *J. Chem. Phys.* **1994**, *101*, 2539.

(7) Nathanson, G. M.; Davidovits, P.; Worsnop, D. R.; Kolb, C. E. *J. Phys. Chem.* **1996**, *100*, 13007.

(8) King, M. E.; Fiehrer, K. M.; Nathanson, G. M.; Minton, T. K. *J. Phys. Chem. A* **1997**, *101*, 6556.

(9) Ringeisen, B. R.; Muenter, A. H.; Nathanson, G. M. *J. Phys. Chem. B* **2002**, *106*, 4988.

(10) Ringeisen, B. R.; Muenter, A. H.; Nathanson, G. M. *J. Phys. Chem. B* **2002**, *106*, 4999.

(11) Manning, M.; Morgan, J. A.; Castro, D. J.; Nathanson, G. M. *J. Chem. Phys.* **2003**, *119*, 12593.

(12) Nathanson, G. M. *Annu. Rev. Phys. Chem.* **2004**, *55*, 231.

(13) Zhang, J.; Garton, D. J.; Minton, T. K. *J. Chem. Phys.* **2002**, *117*, 6239.

(14) Kelso, H.; Kohler, S. P. K.; Henderson, D. A.; McKendrick, K. G. *J. Chem. Phys.* **2003**, *119*, 9985.

(15) Perkins, B. G.; Nesbitt, D. J. *J. Phys. Chem. A* **2010**, *114*, 1398.

(16) Perkins, B. G.; Nesbitt, D. J. *J. Phys. Chem. A* **2009**, *113*, 4613.

(17) Perkins, B. G.; Nesbitt, D. J. *J. Phys. Chem. B* **2008**, *112*, 507.

(18) Perkins, B. G.; Nesbitt, D. J. *J. Phys. Chem. A* **2008**, *112*, 9324.

(19) Perkins, B. G.; Nesbitt, D. J. *Proc. Natl. Acad. Sci. U.S.A.* **2008**, *105*, 12684.

(20) Perkins, B. G.; Nesbitt, D. J. *J. Phys. Chem. A* **2007**, *111*, 7420.

(21) Perkins, B. G.; Nesbitt, D. J. *J. Phys. Chem. B* **2006**, *110*, 17126.

(22) Perkins, B. G.; Haber, T.; Nesbitt, D. J. *J. Phys. Chem. B* **2005**, *109*, 16396.

(23) Wight, A. C.; Miller, R. E. *J. Chem. Phys.* **1998**, *109*, 8626.

(24) Nogueira, J. J.; Vazquez, S. A.; Mazyar, O. A.; Hase, W. L.; Perkins, B. G.; Nesbitt, D. J.; Martinez-Nunez, E. *J. Phys. Chem. A* **2009**, *113*, 3850.

(25) Martínez-Núñez, E.; Rahaman, A.; Hase, W. L. *J. Phys. Chem. C* **2007**, *111*, 354.

(26) Pradeep, T.; Miller, S. A.; Cooks, R. G. *J. Am. Soc. Mass. Spectrom.* **1993**, *4*, 769.

(27) Ramasamy, S.; Pradeep, T. *J. Chem. Phys.* **1995**, *103*, 485.

(28) Nogueira, J. J.; Martinez-Nunez, E.; Vazquez, S. A. *J. Phys. Chem. C* **2009**, *113*, 3300.

(29) Allen, M. P.; Tildesley, D. J. *Computer Simulation of Liquids*; Clarendon Press: Oxford, 1987.

(30) VENUS; VENUS05 is a modified version of VENUS96. (a) Hase, W. L.; Duchovic, R. J.; Hu, X.; Komornicki, A.; Lim, K. F.; Lu, D.-h.; Peslherbe, G. H.; Swamy, K. N.; Vande Linde, S. R.; Varandas, A.; Wang, H.; Wolf, R. *J. QCPE* **1996**, *16*, 671. (b) Hu, X.; Hase, W. L.; Pirraglia, T. *J. Comput. Chem.* **1991**, *12*, 1014.

(31) Lourderaj, U.; Martinez-Nunez, E.; Hase, W. L. *J. Phys. Chem. A* **2007**, *111*, 10292.

(32) Chang, X. Y.; Bintz, K. L.; Thompson, D. L.; Raff, L. M. *J. Phys. Chem.* **1994**, *98*, 6317.

(33) Child, M. S. *Semiclassical Mechanics with Molecular Applications*; Oxford University Press: New York, 1991.

(34) Wilson, E. B.; Decius, J. C.; Cross, P. C. *Molecular Vibrations, The Theory of Infrared and Raman Vibrational Spectra*; McGraw-Hill: New York, 1955.

(35) Bonnet, L.; Rayez, J. C. *Chem. Phys. Lett.* **2004**, *397*, 106.

(36) Bonnet, L.; Rayez, J. C. *Chem. Phys. Lett.* **1997**, *277*, 183.

(37) Banares, L.; Aoiz, F. J.; Honvault, P.; Launay, J. M. *J. Phys. Chem. A* **2004**, *108*, 1616.

(38) Banares, L.; Aoiz, F. J.; Honvault, P.; Bussery-Honvault, B.; Launay, J. M. *J. Chem. Phys.* **2003**, *118*, 565.

(39) Jambrina, P. G.; Aoiz, F. J.; Bulut, N.; Smith, S. C.; Balint-Kurti, G. G.; Hankel, M. *Phys. Chem. Chem. Phys.* **2010**, *12*, 1102.

(40) Brouard, M.; Burak, I.; Marinakis, S.; Minayev, D.; O'Keeffe, P.; Vallance, C.; Aoiz, F. J.; Banares, L.; Castillo, J. F.; Zhang, D. H.; Xie, D.; Yang, M.; Lee, S.-Y.; Collins, M. A. *Phys. Rev. Lett.* **2003**, *90*, 093201.

(41) Grimmelmann, E. K.; Tully, J. C.; Cardillo, M. J. *J. Chem. Phys.* **1979**, *72*, 1039.

(42) Whitnell, R. M.; Wilson, K. R.; Hynes, J. T. *J. Chem. Phys.* **1992**, *96*, 5354.

JP103511G